


Article

# Experimental Evaluation of the Performance of a Three-Phase Five-Level Cascaded H-Bridge Inverter by Means FPGA-Based Control Board for Grid Connected Applications

Fabio Viola 

Dipartimento Energia, ingegneria dell'Informazione e modelli Matematici, DEIM, University of Palermo, 90133 Palermo, Italy; fabio.viola@unipa.it; Tel.: +39-091-238-60253

Received: 22 October 2018; Accepted: 22 November 2018; Published: 26 November 2018



**Abstract:** Over the last decades, plants devoted to the generation of green energy significantly increased their number, together with the demand of same electrical energy, also stored in battery systems. This fact produced the growth of energy conversion systems with advanced performances with respect to the traditional ones. In this circumstance, multilevel converters play a significant role for their great advantages in performances, flexibility, fault-tolerability, employment of renewable energy sources and storage systems and finally yet importantly reduced filter requirements. In this context, this paper faces the performance of a cascaded H-bridge 5 level inverter in terms of harmonic distortion generated and injected into the grid. Through an accurate analysis that takes into account the pulse width modulation (PWM) multicarrier modulation techniques (phase disposition PD, phase opposition disposition POD, alternative phase opposition disposition APOD, phase shifted PS) and related reference signals (sinusoidal reference; third harmonic injection THI reference, switching frequency optimal SFO reference), a framework of distorting harmonics is presented by comparing twelve cases. The results obtained from the simulations are reproduced and validated in a prototype system of five level cascaded H-bridge multilevel inverter. A deep discussion of control and filtering system is provided to justify the choice of the best modulation technique to adopt.

**Keywords:** Cascaded H-bridge multilevel inverter (CHBMLI); field-programmable gate array; total harmonic distortion (THD); modulation techniques

## 1. Introduction

The increased demand of green energy has led to the development of even more performing structures allowing the generation and storage of energy in DC form. The drawbacks are due to the increased number of harmonics introduced and filtered in the power grids.

The three main multilevel power inverter (MPI) structures proposed in technical literature, with their related benefits and disadvantages, according to [1–3] are diode clamped converter (DCC), capacitor-clamped inverter (CCI) and cascaded H-bridge (CHB) multilevel inverter.

The neutral point clamped converter (NPC) was the first multilevel structure proposed. The common DC-link is composed of four capacitors connected in series that split the voltage into four level. The middle point of the capacitors  $n$  is used as neutral point. The peculiar components, that differentiate this circuit from the others multilevel inverters, are the clamping diodes that allow to subdivided the DC voltage on the switches. Thus, the voltage across on the switches is limited to one capacitor voltage equal to  $V_{dc}/(n_L - 1)$ , where  $n_L$  is the number of level. By supposing that for each blocking diode its voltage value is identical to the voltage rating of active device, the number

of diodes requested for each phase will be  $(n_L - 1) \cdot (n_L - 2)$ . This converter presents some operative limits as: (1) max number of levels is five, due both to the complexity of the circuit and both to the large number of components demanded; (2) uneven distribution of semiconductor power losses among the switches, which reduces the switching frequency and the output power; (3) unbalanced capacitor voltages which generate low frequency harmonics; (4) the system cannot involve a modular structure (non-modular topology structure).

Flying capacitor inverters (FCIs) or CCIs are an alternative to overcome some of the DCC disadvantages. The structure of CCIs have similarity to NPC inverter except the CCI uses several capacitors in the place of the clamping diodes. The main advantage of the CCI are the redundant states to obtain the voltage levels. In this way, it is possible an even distribution of semiconductor losses among the switches but it is necessary a dedicated control algorithm to balance the capacitors voltage.

The increase of voltage levels confines the proper charging and discharging mechanism of capacitors. By considering the economical aspect, the cost of the inverter follows the increase of the number of levels, but also the device becomes bulkier and its lifetime decreases due to the growing number of used capacitors. For a  $n_L$ -level converter, it is necessary  $(n_L - 1) \cdot (n_L - 2) / 2$  clamping capacitors per phase in addition to the  $(n_L - 1)$ -main dc bus capacitors. Thus, the high number of capacitors limit the use to three or five levels. Moreover, lack of modularity and high quantity of capacitors for higher number of voltage levels reduces the reliability of this converter.

Figure 1 shows the topology structure of a single-phase five-level cascaded H-bridge multilevel inverter.

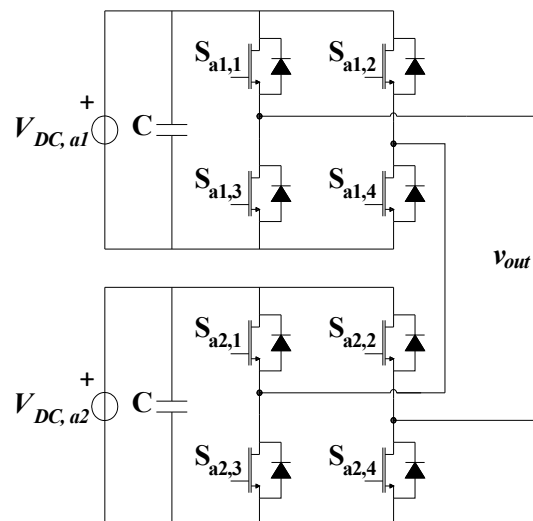


**Figure 1.** Topology structure of a single-phase five-level cascaded H-bridge (CHB) inverter.

This topology has a main advantage: the modular configuration, blocks can be added to reach voltage levels, control is easily performed, and maintenance, in case of fault, requires the disconnection of a block to keep the system working. Thus, each module can be either half- or full-bridge with separated DC source and can be controlled as a single-phase converter. This topology reaches in output medium voltage levels, by enforcing only common low-voltage components so there are not operative limits about max number of the voltage levels. Matching the number of capacitors and diodes between the cited topologies yields that CHB converter has the least number of components.

The phase voltage is synthesized by the addition of the voltages generated by the different modules. Thus, the voltage levels  $n_L$  depend of the number of modules connected in series for phase through the equation:

$$n_L = 2n_{HB} + 1 \quad (1)$$

where  $n_{HB}$  is the number of cells connected in series for phase.

Separated DC sources are an advantage in many applications but this feature leads to a more complex DC-voltage regulation loop.

Others topology structures of multilevel inverters and different classification methods were reported in literature [4]. In [5], an interesting classification into two comprehensive categories according to the applied DC source structure were discussed. A high number of topology structures were developed since separated DC sources are very diffused in renewable energy plants (PV, Wind farm, Fuel cell, etc.).

### 1.1. Overview of Pulse Width Modulation (PWM) Modulation Techniques

Pulse width modulation (PWM) techniques found large use in many industrial applications due to their easy implementation in the modern control systems and the high flexibility. Generally, PWM techniques used for multilevel inverters are an extension of modulation techniques for the traditional two-level voltage source inverters (VSI). A general classification of the modulation strategies for MPI presents two categories: “Fundamental switching frequency” and “High switching frequency”.

Generally, the first category have been used in application where it is necessary to reduce the switching losses (i.e., high power electrical drive) while the second category have been used in applications where it is necessary to reduce the harmonic content on the output voltage (i.e., grid connected systems).

In literature [6–8] were reported many multicarrier modulation PWM methods, which differ for the reference signals and carrier signals. About the carrier signals, there are the “amplitude shifted” multicarrier PWM strategies and the “phase shifted” multicarrier PWM.

Amplitude shifted multicarrier PWM presents three alternative PWM strategies with the identical peak-to-peak amplitude and different phase relationships between the carriers, which are:

- Phase Disposition (PD) (Figure 2a), where all carriers are in phase;
- Phase Opposition Disposition (POD) (Figure 2b), where the carriers above the reference zero point have a difference of phase respect those below the zero point of  $\pi$ ;
- Alternative Phase Opposition Disposition (APOD) (Figure 2c), where each carrier is phase shifted by  $\pi$  from its adjacent carriers.

The carrier number  $n_c$  of the level shifted multicarrier PWM in function of the number of the converter level  $n_L$ , is equal to:

$$n_c = n_L - 1 \quad (2)$$

These strategies lead to elimination of all carriers and related sideband harmonics up to the switching frequency.

Phase shifted multicarrier PWM strategy, shown in Figure 2d, is an extension of the unipolar PWM for traditional single-phase two-level inverter. For this technique, the modulation of the H-bridge inverters in each phase leg is modular. Thus, the reference waveforms for the two-phase legs inverter are phase shifted by  $\pi$ . The number of the carrier signals is equal to  $n_{HB}$  while the phase shifted optimum (PSO) to obtain harmonic cancellation, is achieved:

$$PSO = \frac{(i-1)\pi}{n_{HB}} \quad (3)$$

where  $i$  is the  $i^{th}$  H-Bridge series connected per phase. For a five-level inverter two carrier signals with mutual phase shift equal to  $\pi/2$ , Figure 2b, are necessary. This scheme leads to elimination of all carriers and associated sideband harmonics up to the  $2n_{HB}$  times of the switching frequency.

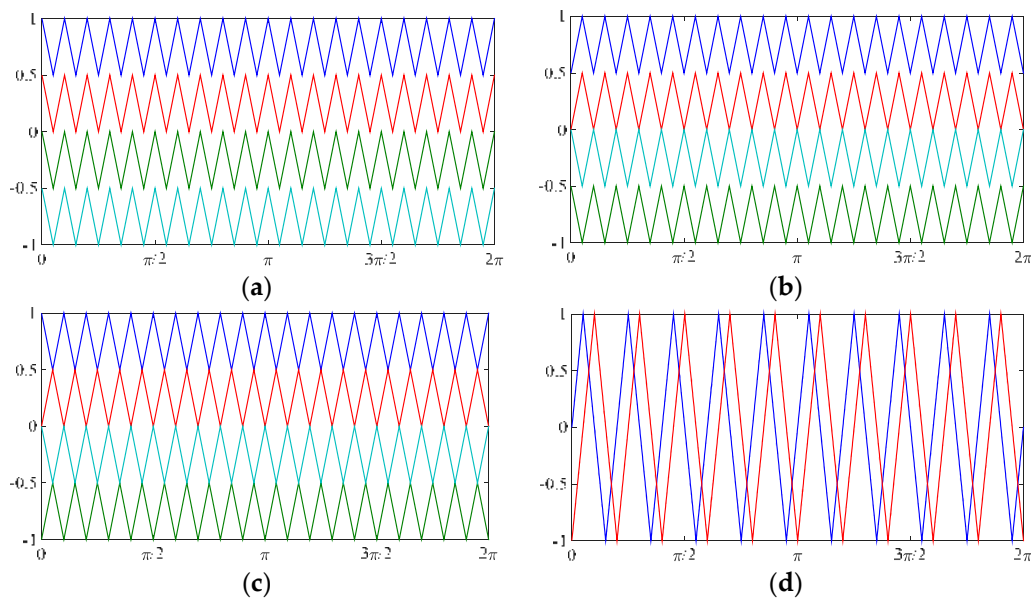


**Figure 2.** Multicarrier strategies for five-level converter: (a) Phase Disposition (PD); (b) Phase Opposition Disposition (POD); (c) Alternative Phase Opposition Disposition (APOD); (d) Phase Shifted (PS). For the first three modulation techniques, four carriers are required, for example in PD technique blue and red lines enable the voltage control of higher bridge, green and cyan the lower bridge. In PS each only two carriers are required since each phase leg has a modular control.

About the reference signals, there are three alternative:

1. Sinusoidal reference;
2. Third harmonic injection (THI);
3. Switching frequency optimal (SFO).

The THI allows overcoming the limit of the three-phase inverters about the reduction of the maximum peak fundamental line voltage of  $\sqrt{3}V_{DC}/2$  (86.60% of  $V_{DC}$ ). Modulation index can be increased by including a common mode third-harmonic term into the reference signal of each phase leg, as shown in Figure 3a (green curve).

This third-harmonic component does not effect on the fundamental line-to-line voltage because the common mode voltages cancel between the phase legs. According to [9], the optimum third-harmonic injection component must have a magnitude of 25% of the fundamental reference. In this way, it is possible to obtain an increasing of the modulation index up to 1.12 and a maximum value of the peak fundamental line-to-line voltage equal to 97% of  $V_{DC}$ .

Figure 3b shows the SFO signal (green curve) for a phase of the converter. As demonstrated in [9], SFO is a space vector equivalent reference voltage that can be used in PWM modulation to produce output voltages with the same average low-frequency content.

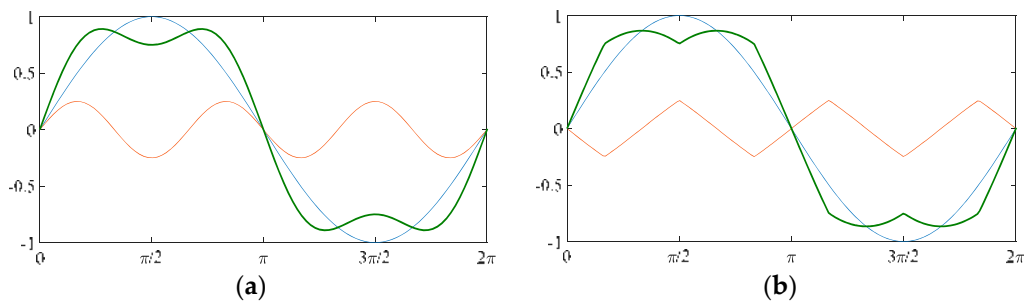


**Figure 3.** Reference signal for a phase of the converter: (a) third harmonic injection (THI); (b) switching frequency optimal (SFO). Blue waveform represents the fundamental, orange is the adjustment signal and blue is the modified reference.

Like the THI, a sinusoidal reference and the three-times-fundamental-frequency triangular reference, called “voltage offset”  $v_{offset}$ , compose SFO reference signal. The mathematical expression of the SFO signal for the three-phase system is:

$$\begin{aligned} v_a^*(t) &= v_a(t) - v_{offset} \\ v_b^*(t) &= v_b(t) - v_{offset} \\ v_c^*(t) &= v_c(t) - v_{offset} \end{aligned} \quad (4)$$

where  $v_a(t)$ ,  $v_b(t)$  and  $v_c(t)$  are the sinusoidal reference that can be expressed in function of the modulation index  $M$  as (5):

$$\begin{aligned} v_a(t) &= M \sin(\omega t) \\ v_b(t) &= M \sin\left(\omega t - \frac{2\pi}{3}\right) \\ v_c(t) &= M \sin\left(\omega t - \frac{4\pi}{3}\right) \end{aligned} \quad (5)$$

The voltage offset  $v_{offset}$  can be expressed as (6):

$$v_{offset} = \frac{\max(v_a, v_b, v_c) + \min(v_a, v_b, v_c)}{2} \quad (6)$$

The arrangement between carrier signals and modulating references produces twelve modulation techniques, graphically summarized in Figures 4–6.

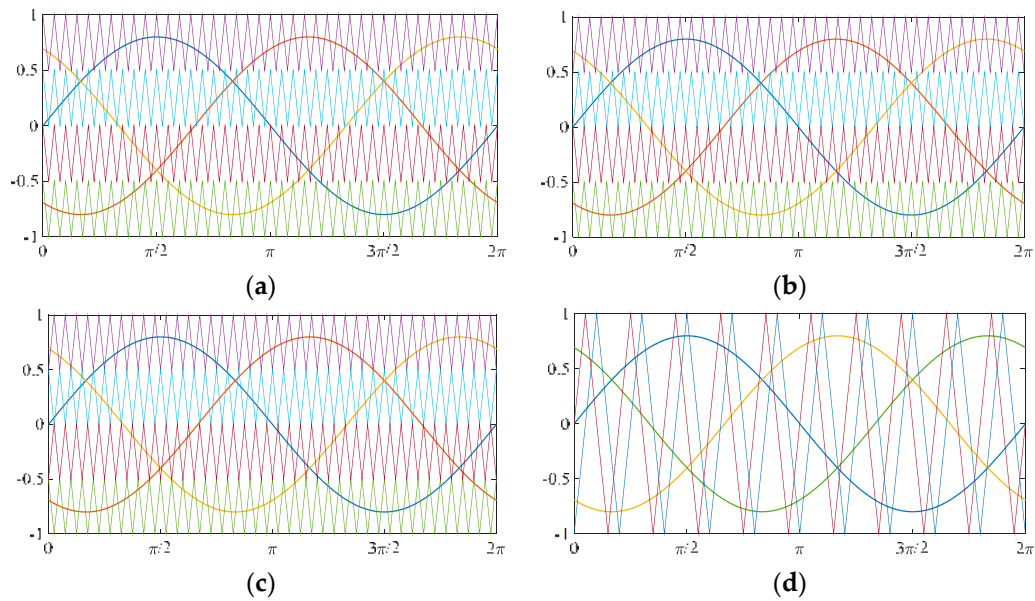


**Figure 4.** Proposed modulation techniques with sinusoidal reference: (a) Phase Disposition (PD); (b) Phase Opposition Disposition (POD); (c) Alternative Phase Opposition Disposition (APOD); and (d) Phase Shifted (PS). Blue, red and orange sinusoidal signals represent the reference signals; interferences with the triangular signals generate the modulation angles for the four switches.

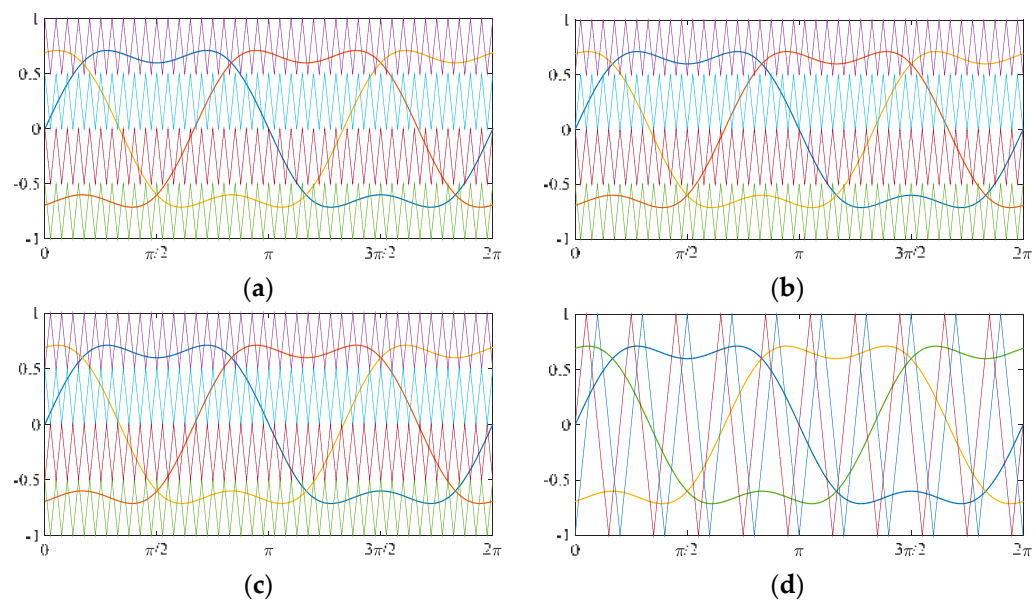


**Figure 5.** Proposed modulation techniques with THI reference: (a) Phase Disposition PD; (b) Phase Opposition Disposition POD; (c) Alternative Phase Opposition Disposition APOD; and (d) Phase Shifted PS. Blue, red and orange THI signals represent the reference signals; interferences with the triangular signals generate the modulation angles for the four switches.

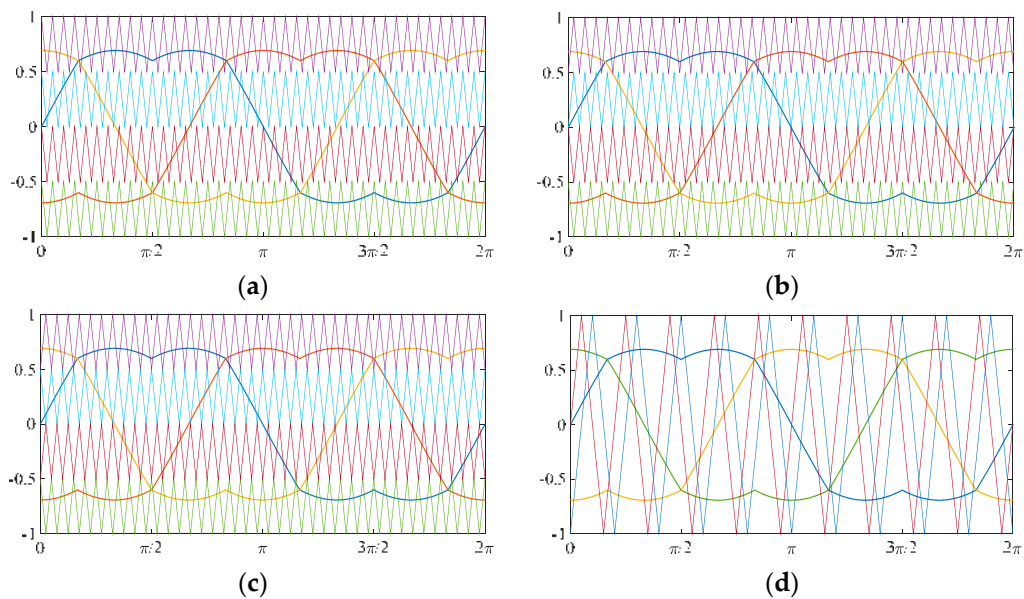


**Figure 6.** Proposed modulation techniques with SFO reference: (a) Phase Disposition (PD); (b) Phase Opposition Disposition (POD); (c) Alternative Phase Opposition Disposition (APOD); and (d) Phase Shifted (PS). Blue, red and orange SFO signals represent the reference signals; interferences with the triangular signals generate the modulation angles for the four switches.

An interesting deep discussion on the previous proposed techniques can be found in [10], in which some features of the proposed technique can be found without the control issue and filter design; preliminary simulations of the multicarrier PWM modulation techniques for a three-phase five-level cascaded H-bridge multilevel inverter (CHBMLI) were also reported in [11,12]. In these works, the authors addressed that the modulation techniques with sinusoidal reference should present the lower values of the total harmonic distortion rate. A complementary study on the use of B-Spline functions as carrier signals replacing triangular waveforms, can be found in [13,14]. This study confirms that the traditional triangle waveforms as carrier signals are solutions that allow best performances.

### 1.2. Digital Control Boards for Power Converters

The fast technological growth of the electronic design automation (EDA) and the very large scale integration (VLSI) has significantly contributed to the development of programmable digital systems with high performances both in terms of execution time and compactness for the realization of control systems. In addition, the recent advances of software for the implementation, simulation and validation of digital systems, dedicated to the control of specific applications, has contributed to simplify and speed-up the overall design process of the digital controller, which represents the core of modern systems for the electrical energy conversion. Figure 7 shows a block diagram of a typical grid-connected system.

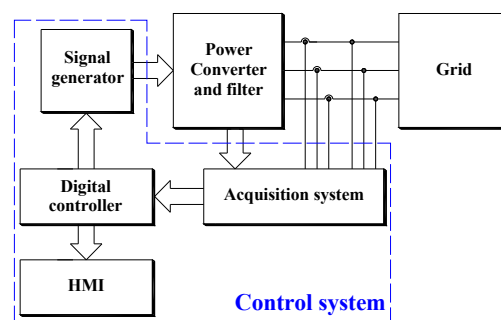


**Figure 7.** Block diagram of a typical grid-connected system. HMI: human-machine interface.

The block named Power Converter and filter requires a control system supervising the behavior (harmonic reduction, filter efficiency, etc.). Generally, the control system consists of four parts:

1. Acquisition system, which provides signal conditioning and digital acquisition of electrical measures (usually current, voltage, frequency) and other quantities (usually solar irradiation, temperature, etc.);
2. Digital controller, required for algorithms employment (filtering, identification, control, modulation of output signals and others);
3. Human-machine interface (HMI), suitable for setup phase as well as for monitoring functions;
4. Signal generator, allowing conversion of the digital signals to analog signals for the power components.

Digital controller represents the core of the control system, different are the digital controller available in the market. A first example of digital controller is the Microcontrollers or DSP (digital signal processor), allowing the implementation of the control algorithms through a purely software programming (with C or C++). The constructor defines the DSP hardware and it is composed by several peripherals, such as the RAM or the ROM. However, an already designed hardware structure reduces the flexibility in the use of the microcontroller. In fact, a complex issue is related to the time of computing of the control algorithm, due to the fact that all the operation needed for this computing are executed in a sequential routine, causing losses in terms of efficiency of the control system [15].

The FPGA (field programmable gate array) is another example of digital controller, composed by a matrix of configurable logic blocks (CLBs) with completely reprogrammable connections. This fact leads to a higher flexibility with respect to a DSP, allowing the realization of specific hardware structures in dependence of the nature of applications. In addition, this feature allows the realization of a system of logic operations developed in parallel, reducing the time of computing. Thus, by means of an FPGA, high-performance control systems can be realized, even comparable with equivalent controllers composed by analogical components, as reported in [16–18].

For instance, the main advantages provided by the adoption of an FPGA-based system for the current control in AC machine drives is presented in [19]. In particular, the FPGA system significantly reduces the execution time of the control algorithm, increasing, therefore, the performances of the related system.

### 1.3. Literature Survey

Research in the world of multilevel inverter is very wide. Different reviews can be found in the literature [20–23], regarding topologies, switching frequencies, employment of photovoltaic sources (PV), control and cost of inverters, depending on different factors such number of sources, switches, and connections.

Novel structures are continuously suggested [24,25] and ways to control them [26–28]. Efficiency, dimension, weight, and reliability influence the cost of manufacturing inverters. Nowadays, multilevel inverters reached in efficiency the value of 98% and the achievement of the next 1% increase is a hard challenge, and ever-more efficient and advanced modulation techniques are required, which are embracing two different ways: low switching frequency modulation techniques and high switching frequency PWM.

Two systems coexist. The main advantage of the employment of the low switching frequency modulation technique is the reduction of the switching losses to a minimum assessment and the confining the stress on the power components (less overshoot). Through one period of the fundamental reference, low switching frequencies techniques generally act one or two commutations of the switches, so generating a staircase waveform. However, the output voltage waveform has different low order harmonics, with amplitudes similar to the fundamental one, hard to be filtered.

Different are the works that face the issue of reducing the harmonics distortion rate (THD) [29–35]. Some of them exploit the problematic of extraction maximum power from PV modules [29] or



implement innovative fast switching modulation, with or without considering power losses [30,31]. As reference, the authors of [32] used a single-phase multilevel inverter scheme, employing three series connected full-bridge stages and a single half-bridge inverter. The result was a reduction of harmonics, evaluated in terms of total harmonic distortion rate, about 9.85%. Spice models help researchers to consider coupled issues such as THD and storage elements [33]. Again, simulation allows the tracking of the performance of a multilevel inverter in partial shaded condition of PV panels [34]. Simulation seems to be the best way to predict how reduce the THD with grid connected systems [35]. The simulation produces a 15-level output voltage, the total harmonic distortion was about 8.12%, a very low level was reached, but similar multilevel inverters will be overpriced.

On the opposite side, higher frequency modulation presents harmonics with higher frequencies, which requires an economic filters, but high frequency switching brings also higher losses due circulating currents. An evaluation of harmonics content, useful to better define the output voltage waveforms, are reported [10–12], and will be objects of deeper discussions in this paper.

High power electrical drives applications need mainly the reduction of the switching losses and electromagnetic interferences (EMI). Losses concur to define efficiency of converter, so soft switching modulation techniques, employing selective harmonic elimination (SHE) technique and selective harmonic mitigation (SHM) technique, are frequently chosen. SHE method requires the choosing of a single  $h^{th}$  harmonic to be removed, so a set of non-linear sinusoidal formulas is solved by choosing the switching angles. The SHM techniques, instead, mitigates simultaneously different harmonics by correctly choosing the switching angles.

Whichever technique is employed, SHE or SHM, to resolve the group of transcendental equations and to discover the related switching angles, different approaches can be taken into account. Obviously, the simplest approach develops iterative methods such as Newton–Rhapson. As reference in [36], the Newton–Rhapson iterative method is employed for the assessment of switching angles for a seven level inverter. The total harmonic distortion of the staircase voltage output is equal to 11.8%.

The authors of [37] present an evaluation between different modulation techniques, applied for a five-level cascaded H-bridge multilevel inverter. The employed control scheme enforces three different pre-defined arrangements for the switching angles. By the uses of these schemes there is an achievement of a minimum THD around 17.07% for the waveform of voltage. The work presented in [38], employs a particularly fast optimal solution of harmonic elimination techniques, used inverter is a five-level multilevel one, and also non-equal DC sources feed the different levels. The solution of the problem is entrusted to a novel particle swarm optimization (PSO) algorithm, and THD achieved a minimum value of 5.44%.

Authors of [39] proposed an optimal SHM technique for a seven-level inverter scheme. The individual harmonic to be mitigated and the THD are subjected to satisfaction of three voltage harmonic standards, named EN50160 [40], CIGRE JWG C4.07 [41] and IEC61000-3-6 [42].

Paper [43] proposes again the PSO technique in presence of PV sources with different voltage levels, the non-linear transcendental equations were solved offline. THD was minimized by employing of pre-calculated switching angles. By the dual employment of the adaptive neuro fuzzy inference system (ANFIS) and also maximum power point tracker (MPPT) algorithm, PV DC sources were transformed in identical DC source. The resulting THD was around 3.7%, less than the ones recommended by IEEE-519 (5%).

Author of [44] again employed an adaptive neuro-fuzzy interference system in order to eliminate voltage harmonics. The proposed comparison shows a best performance of ANFIS referred to neuro fuzzy controller (NFC), in the case of studying a seventh level inverter with active filter. Again the option of an active filter, used in order to improve the performance of the control, can be find in [45].

In [46] the method known as “voltage cancelation” is used for single-phase H-bridge inverters, and in [47] was applied for a single-phase five-level CHBML.

In this paper the structures used in [47] with a soft switching modulation is used with high switching PWM in order to achieve the same or a better THD.

#### 1.4. Contributions and the Organization of Paper

The purpose of this article is to define in detail all the information required to implement the modeling, the operation and the control of a CHBMI.

By starting from general information on CHBMI a detailed report is presented. Informations for the reproduction of the results are not omitted, different tables report the used parameters, from the impedances used in the filtering systems for the various PWM employed techniques (twelve different cases) to the delay times used for driving the system.

Particular attention is devoted to the following aspects: LCL filter design, control design, harmonic content and validation of the proposed approach.

Section 2 is devoted to the simulation of a CHBMI for grid connected applications. The instantaneous model of the converter will be presented in Section 2.1 and after a CHBMI average model. The LCL filter design will be introduced in Section 2.2 and the controller design in Section 2.3. Finally, the simulated performances are evaluated in Section 2.4.

Section 3 is devoted to the experimental validation. The Test Bench will be described in Section 3.1. The control algorithm design will be presented in Section 3.2. The model validation will be discussed in Section 3.3 and finally the grid connected application will be introduced in Section 3.4.

Section 4 recalls and discusses the obtained results, and finally Section 5 concludes the paper.

## 2. Cascaded H-Bridge Inverter for Grid Connected Applications: Modelling and Control

The purpose of this section is to provide all the useful information to realize a virtual model of a CHBMI.

### 2.1. Mathematical Model of the System

Among the classic structures of multilevel inverters presented in literature, this work considers the three-phase, five-level Cascaded H-Bridge inverter topology. Figure 8 shows the topology structure of a three-phase five-level CHB inverter connected to the grid through a LCL filter and a transformer (used for boost voltage and security purpose).

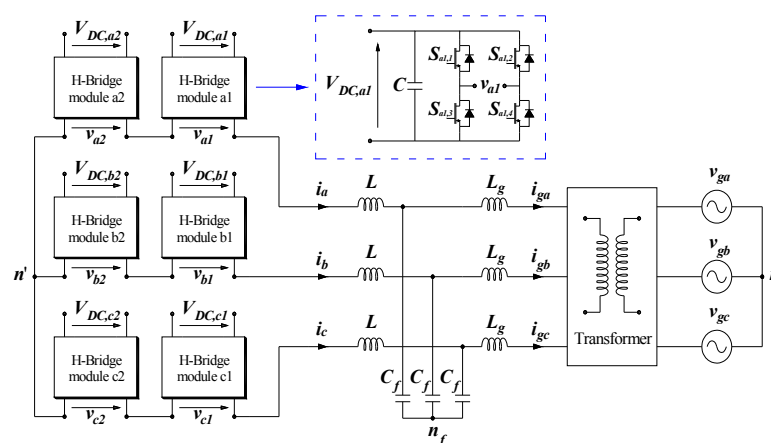


Figure 8. Topology structure of a three-phase five-level CHB inverter system.

Each phase of the CHB inverter consists of two cascaded H-bridges in series connected. Thus, the phase voltages  $v_a(t)$ ,  $v_b(t)$  and  $v_c(t)$ , referred on the  $n'$  point, is obtained by summing output voltage of the series connected H-Bridges (7):

$$\begin{aligned} v_a(t) &= v_{a1}(t) + v_{a2}(t) \\ v_b(t) &= v_{b1}(t) + v_{b2}(t) \\ v_c(t) &= v_{c1}(t) + v_{c2}(t) \end{aligned} \quad (7)$$

Taking into account the switching state of the power components, the instantaneous model of the three-phase five-level CHBMI in both the AC and DC side can be totally described by the following equations:

$$\begin{aligned} v_a(t) &= V_{DC,a1} \cdot (S_{a1,1} - S_{a1,2}) + V_{DC,a2} \cdot (S_{a2,1} - S_{a2,2}) \\ v_b(t) &= V_{DC,b1} \cdot (S_{b1,1} - S_{b1,2}) + V_{DC,b2} \cdot (S_{b2,1} - S_{b2,2}) \\ v_c(t) &= V_{DC,c1} \cdot (S_{c1,1} - S_{c1,2}) + V_{DC,c2} \cdot (S_{c2,1} - S_{c2,2}) \end{aligned} \quad (8)$$

$$\begin{aligned} i_{DC,a1} &= i_a \cdot (S_{a1,1} - S_{a1,2}) & i_{DC,a2} &= i_a \cdot (S_{a2,1} - S_{a2,2}) \\ i_{DC,b1} &= i_b \cdot (S_{b1,1} - S_{b1,2}) & i_{DC,b2} &= i_b \cdot (S_{b2,1} - S_{b2,2}) \\ i_{DC,c1} &= i_c \cdot (S_{c1,1} - S_{c1,2}) & i_{DC,c2} &= i_c \cdot (S_{c2,1} - S_{c2,2}) \end{aligned} \quad (9)$$

$$\begin{aligned} C \frac{dV_{DC,a1}}{dt} &= i_{in,a1} - i_{DC,a1} & C \frac{dV_{DC,a2}}{dt} &= i_{in,a2} - i_{DC,a2} \\ C \frac{dV_{DC,b1}}{dt} &= i_{in,b1} - i_{DC,b1} & C \frac{dV_{DC,b2}}{dt} &= i_{in,b2} - i_{DC,b2} \\ C \frac{dV_{DC,c1}}{dt} &= i_{in,c1} - i_{DC,c1} & C \frac{dV_{DC,c2}}{dt} &= i_{in,c2} - i_{DC,c2} \end{aligned} \quad (10)$$

where  $S_{ji,k}$  ( $j = a \dots c$ ;  $i, k = 1$  or  $2$ ) are the switching state in which “1” represents that the switch is ON and “0” represents that the switch is OFF.

Equations (8) and (9), can be simplified in (12) and (13) by considering the same DC voltage  $V_{DC}$  for each H-Bridges and by defining the switching functions  $S_{ji} \in \{-1, 0, 1\}$  as:

$$S_{ji} = S_{ji,k} - S_{ji,k+1} \quad (11)$$

Thus, Equations (14) and (15) can be rewritten as:

$$\begin{aligned} v_a(t) &= V_{DC} \cdot (S_{a1} + S_{a2}) \\ v_b(t) &= V_{DC} \cdot (S_{b1} + S_{b2}) \\ v_c(t) &= V_{DC} \cdot (S_{c1} + S_{c2}) \end{aligned} \quad (12)$$

$$\begin{aligned} i_{DC,a1} &= i_a \cdot S_{a1} & i_{DC,a2} &= i_a \cdot S_{a2} \\ i_{DC,b1} &= i_b \cdot S_{b1} & i_{DC,b2} &= i_b \cdot S_{b2} \\ i_{DC,c1} &= i_c \cdot S_{c1} & i_{DC,c2} &= i_c \cdot S_{c2} \end{aligned} \quad (13)$$

Equations (12) and (13) represent the instantaneous model of the three-phase five-level CHBMI in terms of the phase voltage and DC current. The line-to-line voltage as described by Equation (14):

$$\begin{aligned} v_{ab}(t) &= V_{DC} \cdot (S_{a1} + S_{a2} - S_{b1} - S_{b2}) \\ v_{bc}(t) &= V_{DC} \cdot (S_{b1} + S_{b2} - S_{c1} - S_{c2}) \\ v_{ca}(t) &= V_{DC} \cdot (S_{c1} + S_{c2} - S_{a1} - S_{a2}) \end{aligned} \quad (14)$$

The model is complete with the equations to describe the LCL filter behavior and the transformer. Thus, the equivalent circuit have to be taken in to account where  $r_{TR}$  and  $L_{TR}$  ( $r_{TR} = 25 \text{ m}\Omega$  and  $L_{TR} = 108.23 \text{ }\mu\text{H}$ ) represent the short-circuit impedance reported on the low side of the transformer.

Finally, the following equations can be used for the rating the output currents  $i_{\{a,b,c\}}$  of the converter (15), grid currents  $i_{g\{a,b,c\}}$  (16) and the capacitor voltages  $v_{\{a,b,c\}}^*$  (17), where  $r$  and  $r_g$  are the resistance of the inductance  $L$  and  $L_g$  of LCL filter.

$$\begin{aligned} L \frac{di_a}{dt} &= v_a - i_a r - v_a^* - v_{nfn'} \\ L \frac{di_b}{dt} &= v_b - i_b r - v_b^* - v_{nfn'} \\ L \frac{di_c}{dt} &= v_c - i_c r - v_c^* - v_{nfn'} \end{aligned} \quad (15)$$

$$\begin{aligned}
(L_g + L_{TR}) \cdot \frac{di_{ga}}{dt} &= v_a^* - i_{ga} \cdot (r_g + r_{TR}) - v_{ga} - v_{nmf} \\
(L_g + L_{TR}) \cdot \frac{di_{gb}}{dt} &= v_b^* - i_{gb} \cdot (r_g + r_{TR}) - v_{gb} - v_{nmf} \\
(L_g + L_{TR}) \cdot \frac{di_{gc}}{dt} &= v_c^* - i_{gc} \cdot (r_g + r_{TR}) - v_{gc} - v_{nmf}
\end{aligned} \tag{16}$$

$$\begin{aligned}
C_f \frac{dv_a^*}{dt} &= i_a - i_{ga} \\
C_f \frac{dv_b^*}{dt} &= i_b - i_{gb} \\
C_f \frac{dv_c^*}{dt} &= i_c - i_{gc}
\end{aligned} \tag{17}$$

where  $v_{n_f n'}$  is the voltage between the point  $n_f$  and  $n'$  and  $v_{nmf}$  is the voltage between the point  $n$  and  $n_f$  that can be expressed by the Equation (18).

$$\begin{aligned}
v_{n_f n'} &= \frac{1}{3} \left[ (v_a + v_b + v_c) - r(i_a + i_b + i_c) - L \left( \frac{di_a}{dt} + \frac{di_b}{dt} + \frac{di_c}{dt} \right) \right] \\
v_{nmf} &= \frac{1}{3} \left[ (v_a^* + v_b^* + v_c^*) - r_g(i_{ga} + i_{gb} + i_{gc}) - L_g \left( \frac{di_{ga}}{dt} + \frac{di_{gb}}{dt} + \frac{di_{gc}}{dt} \right) \right]
\end{aligned} \tag{18}$$

In the case of the equilibration system, the voltage  $v_{nmf}$  is equal to zero. In order to design the control system, it is necessary to develop an average model of the system. Generally, the average model takes into account the average values in a switching period  $T_{sw}$ . In this way, the average phase voltages and average currents can be expressed as (19) and (20):

$$\begin{aligned}
\bar{v}_a(t) &= \frac{1}{T_{sw}} \int_0^{T_{sw}} V_{DC} \cdot (S_{a1} + S_{a2}) dt \\
\bar{v}_b(t) &= \frac{1}{T_{sw}} \int_0^{T_{sw}} V_{DC} \cdot (S_{b1} + S_{b2}) dt \\
\bar{v}_c(t) &= \frac{1}{T_{sw}} \int_0^{T_{sw}} V_{DC} \cdot (S_{c1} + S_{c2}) dt
\end{aligned} \tag{19}$$

$$\begin{aligned}
\bar{i}_{DC,a1} &= \frac{1}{T_{sw}} \int_0^{T_{sw}} i_a \cdot S_{a1} dt & \bar{i}_{DC,a2} &= \frac{1}{T_{sw}} \int_0^{T_{sw}} i_a \cdot S_{a2} dt \\
\bar{i}_{DC,b1} &= \frac{1}{T_{sw}} \int_0^{T_{sw}} i_b \cdot S_{b1} dt & \bar{i}_{DC,b2} &= \frac{1}{T_{sw}} \int_0^{T_{sw}} i_b \cdot S_{b2} dt \\
\bar{i}_{DC,c1} &= \frac{1}{T_{sw}} \int_0^{T_{sw}} i_c \cdot S_{c1} dt & \bar{i}_{DC,c2} &= \frac{1}{T_{sw}} \int_0^{T_{sw}} i_c \cdot S_{c2} dt
\end{aligned} \tag{20}$$

As demonstrated in [46], the equations of the average voltages and average currents in a switching period become (21) and (22):

$$\begin{aligned}
\bar{v}_a(t) &= V_{DC} \cdot (m_{a1} + m_{a2}) \\
\bar{v}_b(t) &= V_{DC} \cdot (m_{b1} + m_{b2}) \\
\bar{v}_c(t) &= V_{DC} \cdot (m_{c1} + m_{c2})
\end{aligned} \tag{21}$$

$$\begin{aligned}
\bar{i}_{DC,a1} &= i_a \cdot m_{a1} & \bar{i}_{DC,a2} &= i_a \cdot m_{a2} \\
\bar{i}_{DC,b1} &= i_b \cdot m_{b1} & \bar{i}_{DC,b2} &= i_b \cdot m_{b2} \\
\bar{i}_{DC,c1} &= i_c \cdot m_{c1} & \bar{i}_{DC,c2} &= i_c \cdot m_{c2}
\end{aligned} \tag{22}$$

where  $m_{ji}$  ( $j = a \dots c$ ;  $i = 1$  or  $2$ ) is the modulation index of each H-Bridge module. Equations (21) and (22) represent the *average model of the converter* in a switching period.

## 2.2. LCL Filter Design

The power quality is an important aspect for grid-connected systems. According to [48,49], there are several limits related to the power injection on the grid that have to be respected, as: voltage unbalance (three-phase inverters should not exceed 3%), DC current injection ( $I_{DC} < 0.5\%$  for IEEE 1574 and  $I_{DC} < 1\%$  for IEC 61727) and current harmonics. The standard harmonic current limits, defined

by IEEE 1574 and IEC 61727 at the point of common coupling (PCC), are summarized in Table 1. Therefore, the level fixed of the total harmonic distortion (THD%) is <5%.

**Table 1.** Current harmonic limits.

Harmonic Order, $h$	Limit in % of Rated Current
$h < 11$	4.0
$11 \leq h < 17$	2.0
$17 \leq h < 23$	1.5
$23 \leq h < 35$	0.6
$h \geq 35$	0.3

On the grid side, a LCL-filter to reduce high-order harmonics that can interfere with other equipment is typically adopted [50]. A step-by-step design procedure for an LCL filter has been proposed in [51,52]. The proposed method employs different factors as inputs such the power rating of the converter, the chosen line frequency and obviously the switching frequency.

According to [52,53], the converter side inductance  $L$  is defined in order to bound the current ripple produced by the converter. Grid side inductance  $L_g^*$  can be determined as a function of  $L$ , using the index  $r$  ( $L_g^* = r \cdot L$ ). While, Capacitor value  $C_f$  can be determined as a percentage  $x\%$  of the delivered reactive power under rated conditions.

Aim of this section is to design the LCL filter parameters with the step-by-step method for each modulation techniques taken into account. The step-by-step procedure was applied by considering a system with a line voltage of 50 V<sub>rms</sub>, frequency 50 Hz and rated power of 600 W (parameters of the test bench in Laboratory of Electrical Applications-LEAP of the University of Palermo).

In Table 2 are reported the converter side inductance  $L$  values for each modulation techniques taken into account. It should be noted that the lower values of  $L$  have been obtained with phase disposition based modulation techniques. Moreover, also phase shifted modulation techniques based present interesting results.

**Table 2.** Grid side inductance values.

	PD	POD	APOD	PS
Sine	0.260 mH	0.882 mH	0.530 mH	0.371 mH
THI	0.222 mH	1.938 mH	0.584 mH	0.393 mH
SFO	0.260 mH	0.882 mH	0.530 mH	0.371 mH

Addition, in the design of the grid side inductance  $L_g^*$  has been taken into account the inductance of the transformer, thus, can be expressed as  $L_g^* = L_g + L_{TR}$ . Table 3 reports the current ripple attenuation depending of the  $r$  and  $x$  values.

**Table 3.** Current Ripple,  $r$  and  $x$  values.

	Sine			THI			SFO		
	$r$	$x\%$	$i_g/i$	$r$	$x\%$	$i_g/i$	$r$	$x\%$	$i_g/i$
PD	1.40	1.94%	10.09%	1.40	2.38%	10.29%	1.20	2.38%	10.03%
POD	0.40	1.94%	10.21%	0.10	3.25%	10.85%	0.40	1.94%	10.21%
APOD	0.90	1.50%	10.81%	0.60	1.94%	10.51%	0.90	1.50%	10.18%
PS	1.00	1.94%	10.21%	1.20	1.50%	10.65%	1.00	1.94%	10.21%

Thus, fixing different values of  $x$  and  $r$ , in particular  $x\%$  less than 5% according to limit reported in [52], have been evaluated the current ripple for each modulation techniques taken into account. In this way, have been identified the values of  $r$  and  $x\%$ , summarized in Table 3, that allow to obtain a

current ripple approximately then 10%. By using the values reported in Table 3, have been calculated the filter parameters and are summarized in Table 4.

**Table 4.** LCL filters parameters and frequency resonant.

	$L$ (mH)	$C_f$ ( $\mu$ F)	$L_g^*$ (mH)	$L_g$ (mH)
SPD	0.260	8.04	0.365	0.257
SPOD	0.882	8.04	0.352	0.244
SAPOD	0.530	6.21	0.477	0.369
SPS	0.371	8.04	0.371	0.263
THIPD	0.222	9.86	0.311	0.203
THIPOD	1.938	13.47	0.193	0.085
THIAPOD	0.584	8.04	0.350	0.242
THIPS	0.393	6.21	0.471	0.363
SFOPD	0.260	9.86	0.313	0.204
SFOPOD	0.882	8.04	0.352	0.244
SFOAPOD	0.530	6.21	0.424	0.316
SFOPS	0.371	8.04	0.371	0.263

An interesting consideration is about the PD based modulation techniques because the converter side inductance  $L$  and grid side inductance  $L_g$  present the lower values. Higher value of the converter side inductance were obtained with THIPOD modulation technique. This phenomenon is attributable at the higher number of the side band harmonics generated by POD carrier signals. In fact, also SPOD and SFOPOD present higher values of the converter side inductance compared others modulation techniques. Regarding the capacitor filter values  $C_f$ , it is interesting to note that have been obtained similar values among the modulation techniques taken into account.

As stated earlier, it is necessary to evaluate the limits on the parameter values, introduced in step-by-step method, to verify the filter effectiveness. In Table 5 are reported the limits on the LCL parameters values for each modulation techniques.

**Table 5.** Limits on the LCL parameter values.

	$\Sigma L$ (p.u.)	$x$ (%)	$f_{res}$ (kHz)
SPD	0.025	1.94%	4.54
SPOD	0.050	1.94%	3.53
SAPOD	0.041	1.50%	4.02
SPS	0.030	1.94%	4.11
THIPD	0.021	2.38%	4.44
THIPOD	0.087	3.25%	3.26
THIAPOD	0.038	1.94%	3.79
THIPS	0.035	1.50%	4.35
SFOPD	0.023	2.38%	4.24
SFOPOD	0.050	1.94%	3.53
SFOAPOD	0.039	1.50%	4.15
SFOPS	0.030	1.94%	4.11

Each LCL configuration designed allows to respect the limits introduced in step-by-step method. In the next section, is reported the design of the control system for each modulation techniques taken into account.

### 2.3. Controller Design

The objective of the control strategy is to guarantee the synchronization with the main grid and regulate the power injection through the current control loop. Moreover, the current loop is accountable of the power quality issues and of protection for high values of current. Thus, low harmonic content on the current and dynamic response are the important properties of the control system.

According to [54–56], the control strategy is based on the synchronous reference frame, also called  $dq$  control. Figure 9 shows the schematic block diagram of the  $dq$  control.

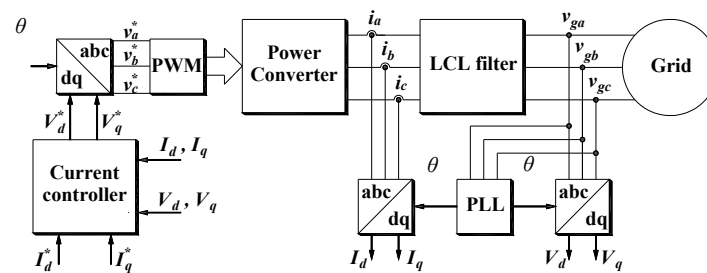


Figure 9. Synchronous reference frame control strategy.

The system needs the measurement of the current and voltage through the sensors. Figure 9 shows that the current sensors are on the converter side, since in more applications they are also employed to protect the power converter. Moreover, the LCL filter design and the control design are influenced by the position of the sensors [51].

Synchronous reference frame control is based on the Park's transformation to express both grid currents and voltages into a reference structure rotating synchronously with the grid frequency. In this way, the  $dq$  components of the voltage and current assume continuous trend and it is possible to use the PI regulator.

The phase-locked loop (PLL) technique [55], allows extracting the instantaneous phase angle of the grid voltage in order to synchronize the voltage waveforms.

For the control design, the instantaneous model of the system, Equations (15) and (16), can be simplified neglecting the filter capacitor  $C_f$ .

Using the Park's transformation, the Equations (15) and (16) can be rewritten as (23):

$$\begin{aligned} v_d(t) &= r_T i_d(t) + L_T \frac{di_d(t)}{dt} - \omega_g L_T i_q(t) + v_{gd}(t) \\ v_q(t) &= r_T i_q(t) + L_T \frac{di_q(t)}{dt} + \omega_g L_T i_d(t) + v_{gq}(t) \end{aligned} \quad (23)$$

where  $r_T$  is the sum of the internal resistance of the inductors ( $r_T = r + r_g + r_{TR}$ ) and the  $L_T$  is the sum of the inductance of the LCL filter and the short-circuit inductance reported on the low side of the transformer ( $L_T = L + L_g + L_{TR}$ ).

In synchronous reference frame, it is possible to control the  $dq$  components independently thanks the decoupling of the two-channel control. In this way, through the  $d$  component it is possible to control the active power while through the  $q$  component it is possible to control the reactive power.

For the design of the proportional-integral (PI) regulators, the method used to tune the parameters of the PI is the "technical optimum" criterion where both plant and PI regulator have the same time constant in order to simplify the closed loop transfer function.

By according the PI integrator time constant  $T_I$  equal to the plant time constant  $T_I = L_T/r_T$ , with the aim to delete the slower plant pole and supposing a perfect pole-zero cancellation, the current closed-loop transfer function  $W(s)$  become of the second order Equation (24).

$$W(s) = \frac{k_p}{s^2 + \frac{1}{1.5T}s + \frac{k_p}{1.5L_T T}} \quad (24)$$

where  $k_p$  is the proportional gain,  $T_I$  is the integral time constant and  $T$  is the sampling period.

By the analysis of Equation (24), the proportional gain  $k_p$  depends on the inductance of the LCL filter. In this way, it is possible to evaluate the PI regulators parameters for each modulation techniques choosing a damping coefficient equal to 0.707. In Table 6 are reported the PI regulator parameters for each modulation techniques taken into account.

**Table 6.** PI regulator parameters.

	Sine			THI			SFO		
	$k_p$	$T_I$ (ms)	$k_i$	$k_p$	$T_I$ (ms)	$k_i$	$k_p$	$T_I$ (ms)	$k_i$
PD	2.09	15.65	133.73	1.78	13.36	133.73	1.91	14.35	133.73
POD	4.12	30.88	133.73	7.11	53.31	133.73	4.11	30.88	133.73
APOD	3.36	25.20	133.73	3.12	23.36	133.73	3.18	23.87	133.73
PS	2.48	18.58	133.73	2.88	21.63	133.73	2.48	18.58	133.73

In the next section, simulation results were reported to evaluate the performance of the system with each modulation techniques taken into account.

#### 2.4. Performances Evaluation

Aim of this section is to evaluate the performance of the system through a simulation analysis for each modulation techniques taken into account. In particular, the main purpose is to investigate the effectiveness of the control strategy and the LCL filter in terms of the harmonic content in the currents and voltages in order to determinate the best solution for grid connected applications. The simulation have been carried out in Matlab/Simulink<sup>®</sup> (version 4.1.1, The MathWorks, Inc., Natick, MA, USA) environment with the same parameters used for each modulation techniques taken into account and reported in Table 7.

**Table 7.** Simulation parameters.

Electric parameter	Value
Grid line Voltage	50 V
Rated current	6 A
Grid frequency	50 Hz
DC Voltages	24 V
Switching frequency	10 kHz
Inductance and resistance of the transformer (low side reported)	108.23 $\mu$ H 25 m $\Omega$

LCL filter requirements and parameters of regulators were determined in the precedent sub-sections (2.2. LCL Filter Design and 2.3. Controller Design). In the follow are reported the results obtained in simulation analysis for each modulation techniques taken into account and have been compared the results among the modulation with the same carrier signals.

##### 2.4.1. Phase Disposition

Generally, the main characteristics of the modulation techniques with PD as carrier signals is that the harmonic spectra of the phase voltage presents a predominant harmonic centered on the switching frequency and side band harmonics. Thus, the difference among SPD, THIPD, and SFOPD are in the amplitude on the harmonic centered on the switching frequency and side band harmonics as shown in Figure 10. However, THI and SFO introduce a third harmonic component on the phase voltage that disappear on the line voltage (three-wired systems).

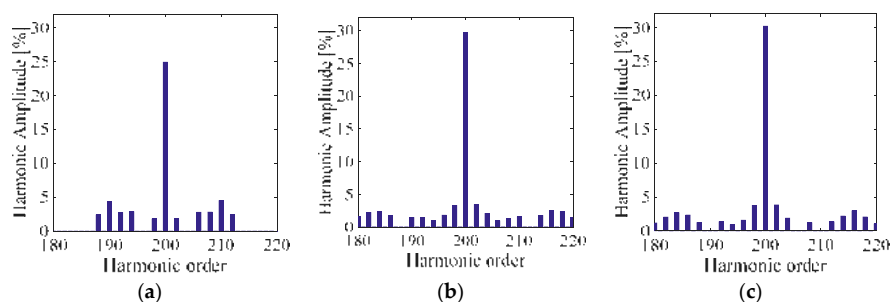


**Figure 10.** Phase voltage harmonic spectra centered around the switching frequency (10kHz) in percent respect to the fundamental amplitude of (a) SPD, (b) THIPD and (c) SFOPD.



This phenomenon explains the different values of THD% and different LCL filter requirements. Consequently, the performance in terms of the harmonic content on the current will be different. Figures 11–13 show the transitory of the converter side currents and grid side currents from zero to the rated current obtained with SPD, THIPD, and SFOPD, respectively. As mentioned above, are visible little differences in the currents trend among SPD, THIPD, and SFOPD, as emphasized by red and green zoom windows. In particular, these differences are present in terms of harmonic content around the switching frequency and the low order harmonics.

Overall, the three-grid side current have a total harmonic distortion—THD% less than 5% according to IEEE 1574 and IEC 61727.

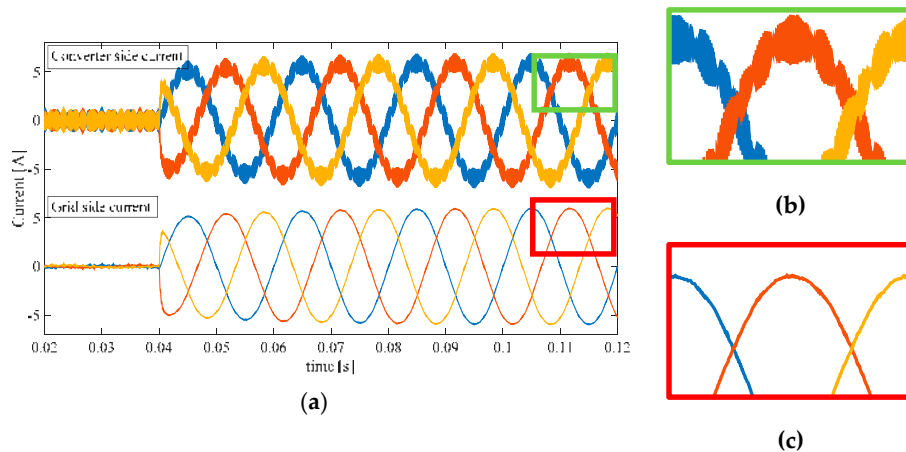


**Figure 11.** Converter side and grid side three-phase current with SPD. (a) Transient behavior in multiple cycles; (b) Ripple magnification for converter side current; (c) Ripple magnification for grid side current.

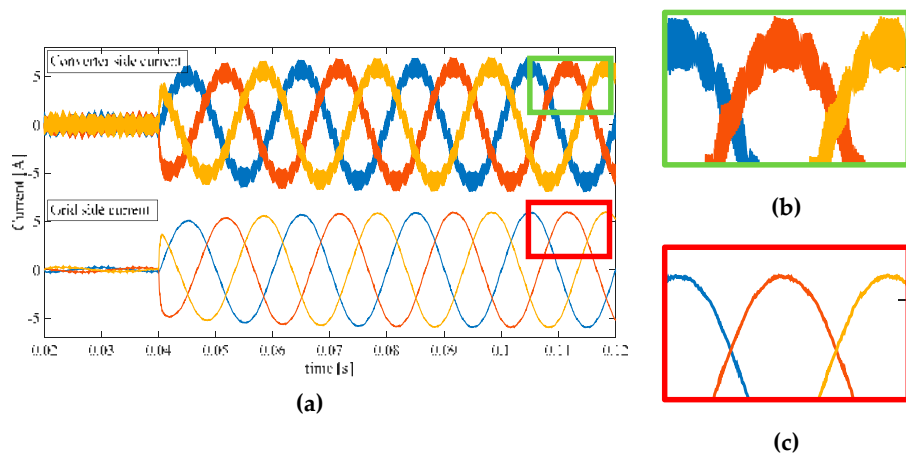


**Figure 12.** Converter side and grid side three-phase current with THIPD. (a) Transient behavior in multiple cycles; (b) Ripple magnification for converter side current; (c) Ripple magnification for grid side current.